

Reprinted from

JAPANESE JOURNAL OF
**APPLIED
PHYSICS**

REGULAR PAPER

**Experimental Study on Surface-Orientation/Strain Dependence
of Phonon Confinement Effects and Band Structure Modulation
in Two-Dimensional Si Layers**

Tomohisa Mizuno, Takashi Aoki, Yuhsuke Nagata, Yuhta Nakahara, and Toshiyuki Sameshima

Jpn. J. Appl. Phys. **52** (2013) 04CC13

Experimental Study on Surface-Orientation/Strain Dependence of Phonon Confinement Effects and Band Structure Modulation in Two-Dimensional Si Layers

Tomohisa Mizuno^{1*}, Takashi Aoki¹, Yuhsuke Nagata¹, Yuhta Nakahara¹, and Toshiyuki Sameshima²

¹Department of Science, Kanagawa University, Hiratsuka, Kanagawa 259-1293, Japan

²Department of Engineering, Tokyo University of Agriculture and Technology, Koganei, Tokyo 184-8588, Japan

E-mail: mizuno@info.kanagawa-u.ac.jp

Received September 7, 2012; revised November 30, 2012; accepted December 11, 2012; published online March 21, 2013

We have experimentally studied the surface orientation/strain effects on quantum mechanical confinement (QMC) in two-dimensional (2D) Si layers with thicknesses less than the Si lattice constant for future metal–oxide–semiconductor (MOS) devices. By UV–Raman spectroscopy, we have demonstrated that the quantum phonon confinement effects (PCEs) rapidly increase with decreasing 2D Si thickness T_S , but is almost independent of surface orientation and strain. Thus, electron saturation velocity of the 2D Si is degraded by the reduced phonon energy owing to the PCEs. On the other hand, photoluminescence (PL) emitted from the only (100)-surface 2D Si layers, depends on the excitation photon energy $h\nu$ ($2.33 \leq h\nu \leq 3.81$ eV), and PL intensity increases with decreasing T_S . The PL data can be explained by simple PL models considering the electron/hole pair recombination mechanism. Consequently, it is necessary to reconstruct the device design for future Si devices, considering the T_S dependence of the 2D Si properties. © 2013 The Japan Society of Applied Physics

1. Introduction

Two-dimensional (2D) Si structures are widely used for extremely thin silicon-on-insulator (ETSOI) field-effect transistors (FETs) and 3D metal–oxide–semiconductor (MOS) devices, such as FinFETs,¹ as well as Si photonic devices.^{2,3} To improve the short-channel effects (SCEs) of MOSFETs and photoluminescence (PL) intensity of Si photonic devices, the 2D Si thickness T_S should continue to be scaled down.^{1–3} However, the quantum confinement effects (QCEs) in a thinner T_S structure cause electron mobility modulation,^{4–6} which is due to the QCEs of 2D electrons in ETSOIs. In addition, the QCEs induce band structure modulation, resulting in the band gap E_G expansion of ETSOIs.^{7–9}

On the other hand, the first-order Raman scattering phonon energy is the longitudinal optical phonon (LO) energy ($E_{P0} \sim 64$ meV) at $\mathbf{q} \approx 0$ (Γ point in the Brillouin zone), where \mathbf{q} is the wave vector of the scattered phonons.¹⁰ However, in a low-D Si structure, the finite Si size effects cause the quantum \mathbf{q} uncertain Δq ; thus, Δq relaxes the momentum conservation and the first-order Raman selection rule in the phonon dispersion curve, which is attributable to allowing the participation of phonons away from the Γ point.^{11–17} As a result, the Raman peaks of wave number less than 520 cm^{-1} become active in the low-D Si; thus, the phonon confinement effects (PCEs) cause a downshift and an asymmetric broadening of the Raman peak.^{11–14,17} The PCEs are reported to be enhanced in 1D and 0D Si semiconductors, such as Si nanowires (1D)^{12,17} and nanocrystals (0D),^{12,16} compared with those in ETSOIs, because Δq increases with decreasing Si dimension from 2D to 0D. In the case of 2D Si, the finite Si thickness causes the phonon wave vector uncertainty, resulting in the PCEs in 2D Si. Therefore, the PCEs induce carrier mobility reduction owing to the enlarged phonon scattering of carriers even in ETSOIs.¹⁸ Moreover, the drain current drivability of the 2D Si devices is also degraded by the self-heating effects in the ETSOI structures.¹ Therefore, it is very important to study

the 2D phonon properties as well as modulated band structures in the 2D Si layer, to clarify both the phonon induced carrier velocity reduction and thermal property (such as thermal conductivity) of the 2D Si structures.

On the other hand, the QCEs are reported to modulate the 2D Si band structures, and thus, to change the Si crystals to a direct band-gap material from an indirect band-gap 3D Si.^{3,7,18,19} In addition, even in the Si material, PL has been observed in low-dimensional porous-Si (p-Si),²⁰ polycrystalline Si,²¹ and even thin-film Si,^{3,19,22,23} which is caused by strong QCEs. In particular, it is also reported that the T_S dependence of peak photon energy is caused by the direct optical transmission in the direct band-gap thin-film Si material that is changed from the indirect band-gap bulk Si material.¹⁹

Recently, we have experimentally demonstrated the PCEs even in a (100) 2D Si unit cell layer with $T_S \approx a$ (Si monolayer), where a is a Si lattice constant of 0.543 nm .²⁴ The surface orientation engineering and strain technique have been the major technologies for realizing high-performance complementary MOS (CMOS) devices,¹ but their influence on the QMCs in 2D Si structures has not been studied in detail, yet.

In this work, for the first time, we have experimentally studied the surface orientation and tensile strain effects on both the PCEs and the PL results of the 2D Si unit cell layer with the minimum T_S of $a/2$. We have also analyzed the 2D phonon properties.²⁵ We have shown the enhancement of both the PCEs evaluated by UV–Raman spectroscopy and PL intensity of $T_S < 1\text{ nm}$, and also discussed the physical properties of 2D Si structures, such as the carrier saturation velocity v_{SAT} , and the band structure modulation.

2. Experimental Procedure for Various 2D Si Layers

2D Si structures were fabricated by a usual thermal dry oxidation of bonded (100)-SOI, (110)-SOI, and (100)-strained SOI (SSOI) substrates²⁶ at a high temperature T (1000°C). The initial T_S in all substrate structures is $16\text{--}80\text{ nm}$, and the initial biaxial strain value of SSOIs is 0.7% .

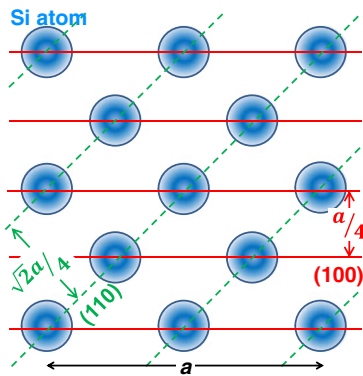


Fig. 1. (Color online) Schematic Si unit cell with lattice constant of a ($\equiv 0.543$ nm) projected onto the (100) plane. The solid and the dashed lines also show the (100) and the (110) Si layers projecting on the (100) plane, respectively. The minimum distance between Si atom layers at the (100) (solid lines) and the (110) (dashed lines) surfaces are $d_{100} \equiv a/4$ ($\equiv 0.136$ nm) and $d_{110} \equiv \sqrt{2}a/4$ ($\equiv 0.192$ nm), respectively.

Therefore, the three substrates have $\text{SiO}_2/\text{Si}/\text{buried-oxide}$ quantum well structures, and the thickness of the surface SiO_2 T_{OX} in the 2D Si is larger than several ten nm, and the buried oxide (BOX) T_{BOX} is about 150 nm.

High-resolution transmission electron microscopy (HRTEM) observations show that high crystal quality can be achieved even in 2D Si layers at T_{S} of less than 0.6 nm, and no amorphous Si (a-Si) region was observed in the whole 2D Si layer.²⁴⁾ The T_{S} of 2D Si layers is mainly evaluated from UV/visual reflection spectra, which is also verified by HRTEM.²⁴⁾

We evaluated the PCEs of the 2D Si layers by UV (325 nm He–Cd laser) Raman spectroscopy and the PL spectra as a function of an excitation laser photon energies $h\nu$ of 2.33 eV (wavelength $\lambda = 532$ nm), 2.81 eV ($\lambda = 441$ nm), and 3.81 eV ($\lambda = 325$ nm) at room temperature, where h is Planck constant and ν is the photon frequency. In this work, the laser diameter is 1 μm , and the laser penetration lengths λ_{P} of 532, 441, and 325 nm in the 3D Si layer are about 1000, 500, and 5 nm, respectively. The laser power is 1 mW, to compress the Raman peak downshift due to the laser power heating effects¹⁷⁾ on the 2D Si layer, as discussed in Sect. 3.1.

3. Results and Discussion

3.1 Phonon confinement effects in 2D Si

Figure 1 shows a schematic of Si unit cell projected onto the (100) plane. The minimum distance d between Si atom layers at the (100) (solid lines) and (110) (dashed lines) surfaces are $d_{100} \equiv a/4$ ($\equiv 0.136$ nm) and $d_{110} \equiv \sqrt{2}a/4$ ($\equiv 0.192$ nm), respectively. In this work, the d of (100)-SSOI is also equal to d_{100} . As a result, it is expected that the physical properties of the 2D Si structures strongly depend on the surface orientation, because $d_{100} \neq d_{110}$.

Figure 2(a) shows the Raman peak intensity I_{P} as a function of T_{S} of the (100)-SOI, (110)-SOI, and (100)-SSOI substrates. It is clear that I_{P} in all substrates rapidly increases with decreasing T_{S} , which is probably due to the resonant Raman scattering in 2D Si structures.²⁷⁾ In addition, only (110)-SOI shows the T_{S} dependence of I_{P} shifting toward the thicker T_{S} region, whereas the (100)-SOI and the (100)-SSOI

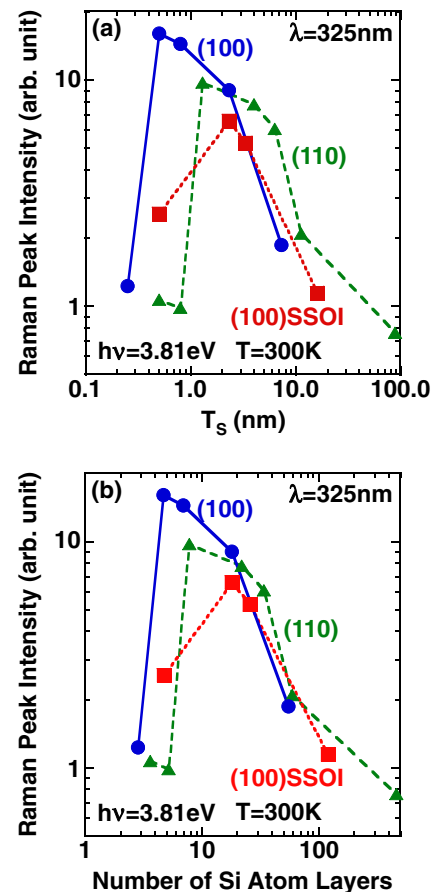


Fig. 2. (Color online) Resonant UV–Raman scattering effects on Raman peak intensity as a function of (a) T_{S} and (b) N_{L} of (100) Si ($\equiv T_{\text{S}}/d_{100}$), (110) Si ($\equiv T_{\text{S}}/d_{110}$) and (100) s-Si layers ($\equiv T_{\text{S}}/d_{100}$), where He–Cd laser wavelength is 325 nm. The circles, triangles, and squares show the experimental data of the (100)-SOI, (110)-SOI, and (100)-SSOI, respectively. (a) shows that I_{P} in the 2D Si layer increases with decreasing T_{S} and N_{L} , which is caused by the band gap modulation of the 2D Si layer. However, I_{P} rapidly decreases at $T_{\text{S}} \leq 0.5$ nm, which is attributed to the rapid decrease in T_{S} . On the other hand, (b) shows that all substrate structures have the universal N_{L} dependence of I_{P} at $N_{\text{L}} > 10$.

show the same T_{S} dependence of I_{P} . Here, the number of Si atom layers N_{L} is defined by $N_{\text{L}} \equiv T_{\text{S}}/d + 1$, where d is the minimum distance between Si atom layers, as shown in Fig. 1. Figure 2(b) also shows the N_{L} dependence of I_{P} , where the N_{L} of the (100)-SOI, (110)-SOI, and (100)-SSOI are $T_{\text{S}}/d_{100} + 1$, $T_{\text{S}}/d_{110} + 1$, and $T_{\text{S}}/d_{100} + 1$, respectively. When $N_{\text{L}} \geq 10$, the N_{L} dependence of I_{P} is independent of surface orientation; thus, all the 2D Si structures show the universal N_{L} dependence of I_{P} . Therefore, the N_{L} dependence instead of the T_{S} dependence is the better indicator for evaluation of the Raman characteristics of 2D Si. Thus, in this section, we discuss the N_{L} dependence of Raman characteristics. The enhanced resonant Raman scattering effects suggest that the band-gap modulation at the Γ point is enhanced with decreasing T_{S} and N_{L} in the 2D Si structures. On the other hand, I_{P} rapidly decreases at $T_{\text{S}} \leq 0.5$ nm and $N_{\text{L}} \leq 5$, which is attributed to the rapid decreases of T_{S} and N_{L} values. Consequently, since the Raman Si intensity under the BOX layer is very low, compared with I_{P} of 2D Si layers, it is possible to evaluate the Raman spectroscopy of 2D Si layers precisely even at $T_{\text{S}} < 1$ nm and $N_{\text{L}} < 10$.

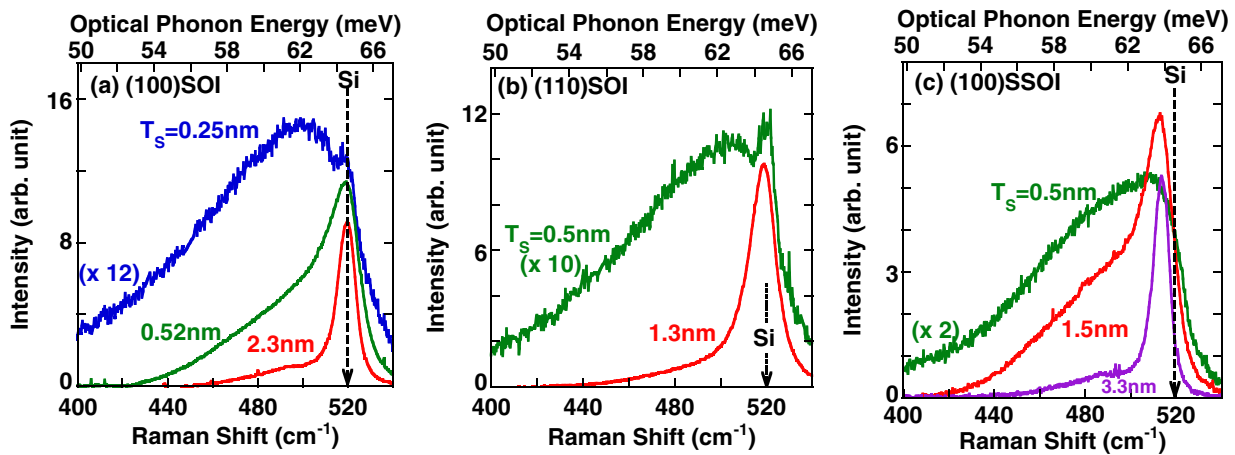


Fig. 3. (Color online) UV-Raman spectra of (a) (100)-SOI, (b) (110)-SOI, and (c) (100)-SSOI substrates at various 2D Si thicknesses T_S . The upper and lower axes show the optical phonon energy $E_P (\equiv hc\omega)$ and wave number ω of Raman shift, respectively, where c is the speed of light. Asymmetrical broadening and downshift of Raman peaks increases with decreasing T_S in all substrate structures.

Next, Fig. 3 show the UV-Raman spectra I_R of (100)-SOI, (110)-SOI, and (100)-SSOI, respectively. The upper axis shows the optical phonon energy $E_P (\equiv hc\omega)$, where c is the speed of light in vacuum and ω is wave number of Raman shift. When $T_S < 5$ nm, we observed the asymmetric broadening of Raman line shapes and the peak downshift $\Delta\omega$ from the usual 3D Si Raman peak (520 cm^{-1}) in all Si substrates, which are attributable to the PCEs in the 2D Si layers.²⁴ These Raman data of the 2D Si are similar to those of 1D and 0D Si structures.^{12–14,17} $\Delta\omega$ is attributable to the decrease in the E_P values in 2D Si layers and most E_P values of 2D Si layers are lower than 3D Si E_P of 64 meV.¹⁰ The PCEs of both the asymmetric broadening and the $\Delta\omega$ are enhanced with decreasing T_S , and becomes very large especially in 0.25 nm (100)-SOI, 0.5 nm (110)-SOI, and 0.5 nm (100)-SSOI. Thus, for the first time, we have experimentally demonstrated the PCEs even in (110)-SOI and (100)-SSOI structures. Moreover, the second peaks of 0.25 nm (100)-SOI and 0.5 nm (110)-SOI at 520 cm^{-1} are attributable to the Si intensity under the BOX layer I_{RB} , but are only 2% of the integrating Raman intensity distribution $\int I_R(\omega) d\omega$, where $I_R(\omega)$ is the Raman intensity distribution. Therefore, we confirmed that the influence of I_{RB} on Fig. 3 data is very small, because of the resonant Raman scattering effects, as shown in Fig. 2. This is also verified by the (100)-SSOI spectra data that the clear Raman peak of the 3D Si layer under the BOX does not exist even in $T_S < 3$ nm, as shown in Fig. 3(c).

The Raman spectra of the Si nanowires and nanocrystals with a high heat resistance strongly depend on the Raman laser power P_L .¹⁷ Here, we discuss the P_L dependence of the Raman spectrum of 2D Si layers. Figure 4 shows the Raman peak downshift $\Delta\omega$ of the (100) 2D Si from 520 cm^{-1} , where $T_S = 0.5$ nm. As shown in Fig. 4, when $P_L > 1$ mW, $\Delta\omega$ increases slightly, which is probably due to the self-heating of the 2D Si layer caused by laser power. However, when $P_L \leq 1$ mW, $\Delta\omega$ is almost independent of P_L . Therefore, the influence of P_L on the Raman spectrum of 2D Si layers is considered to be small in our study, when $P_L \leq 1$ mW.

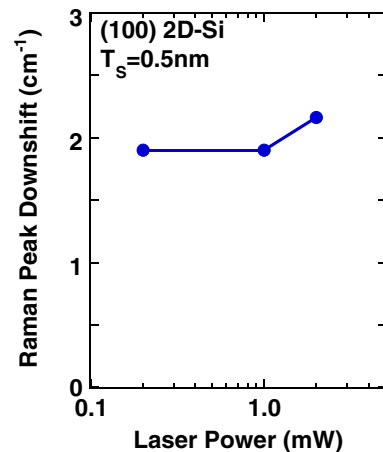


Fig. 4. (Color online) Laser power P_L dependence of Raman peak downshift $\Delta\omega$ of (100) 2D Si, where $T_S \approx 0.5$ nm. $\Delta\omega$ remains constant, when $P_L \leq 1$ mW.

The Raman line shapes of the 2D Si layers are irregular, as shown in Fig. 3; thus, the asymmetric broadening cannot be evaluated from the usual full width at half maximum (FWHM) of the Raman peaks. Therefore, to analyze the asymmetric broadening, we introduce two parameters¹² of wave number width of the asymmetrical Raman peaks, shown as W_L and W_H in Fig. 5(a). Figure 5(a) shows the asymmetrical broadening of Raman spectrum of (110) 2D Si, where $T_S \approx 0.5$ nm ($N_L \approx 3$). W_L and W_H are defined by width at the tenth maximum of the Raman peak intensity in the lower and higher wave number regions from 520 cm^{-1} of the Γ point E_{P0} , respectively. In the case of a thicker Si layer without the PCEs, it is expected that $W_L = W_H$, and thus W_L or W_H is also an indicator for the Si crystal quality, because the Raman line shapes of the thicker Si layer can be expressed by the symmetrical Lorentzians. Figures 5(b) and 5(c) show the N_L dependence of W_L and W_H of the Raman peaks, respectively, where circles show (100)-SOI, triangles (110)-SOI, and squares (100)-SSOI. When $N_L < 20$ ($T_S < 3$ nm), W_L rapidly increases with decreasing N_L , resulting in $W_L \gg W_H$. W_L at $N_L \approx 3$ in the (100)-SOI amounts to about

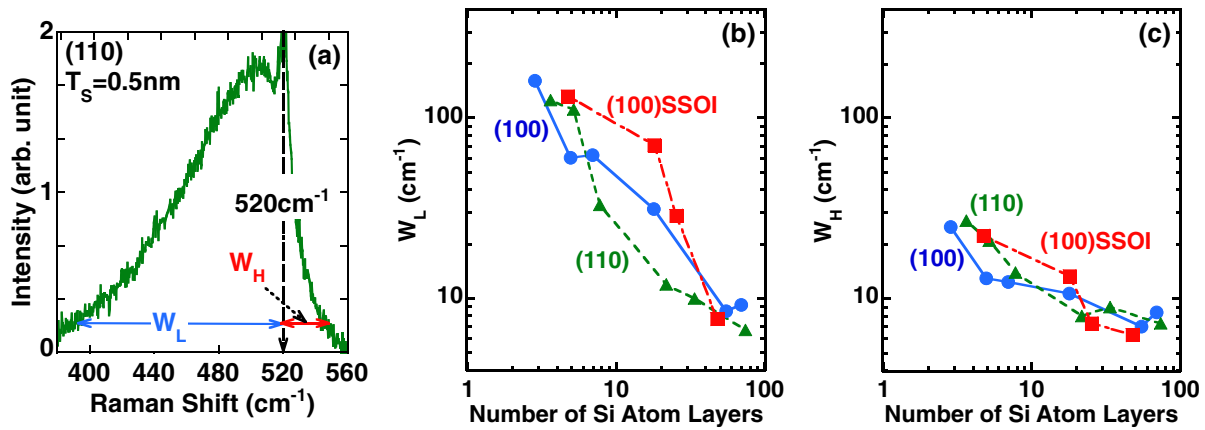


Fig. 5. (Color online) (a) Asymmetrical broadening of Raman spectrum of (110) 2D Si, where $T_S \approx 0.5$ nm ($N_L \approx 3$). W_L and W_H are defined by the width at the tenth maximum of the Raman peak value in the low and high wave number regions from 520 cm^{-1} , respectively. N_L dependence of (b) W_L and (c) W_H of the Raman peaks of (100)-SOI (circles), (110)-SOI (triangles), and (100)-SSOI (squares). When $N_L < 20$, W_L rapidly increases with decreasing N_L . However, when $N_L > 20$, W_L is almost the same as the W_H , because of the PCEs reduction in thick Si structures. The (100) and (110) 2D Si structures have the almost universal N_L dependence of W_L and W_H .

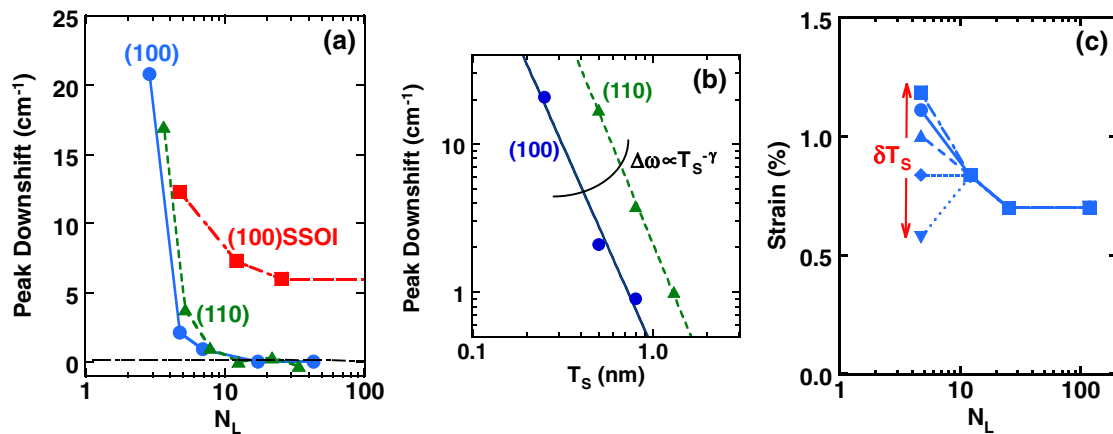


Fig. 6. (Color online) (a) N_L dependence of Raman peak downshift $\Delta\omega$ of (100)-SOI (circles), (110)-SOI (triangles), and (100)-SSOI (squares) from 3D Si peak (520 cm^{-1}). When $N_L < 10$, $\Delta\omega$ rapidly increase with decreasing N_L in all substrates. Moreover, the (100) and (110) 2D Si structures have the universal N_L dependence of $\Delta\omega$. (b) T_S dependence of Raman peak downshift $\Delta\omega$ of (100)-SOI (circles) and (110)-SOI (triangles), where $N_L < 8$. $\Delta\omega$ in both (100) and (110) 2D Si can be well fitted by the power law of T_S with the correlation coefficient of about 0.998. (c) N_L dependence of the strain ε of SSOIs estimated by subtracting the $\Delta\omega$ values of (100)-SOI obtained by Eq. (1) from the experimental $\Delta\omega$ values of (100)-SSOI. At $N_L \approx 4$, the T_S variation δT_S (0.2 nm in this study) leads to ε variation; thus, the ε behavior at $N_L \approx 4$ is not clear at present. However, the strain value is independent of N_L , when $N_L > 10$.

15 times as large as that of thicker Si layers. However, when $N_L > 30$, W_L is almost independent of N_L and is almost the same as W_H , because the PCEs are very small in the thicker Si structures. Therefore, the lower W_H values of at least $N_L > 30$ indicate good Si crystal quality. These results are consistent with the ETSOI data with $T_S \geq 5$ nm reported by Uchida et al.⁵⁾ However, W_H at $N_L < 20$ is also modulated by PCEs; thus, it is difficult to analyze the Si crystal quality, using W_H . In addition, the (100) and (110) 2D Si structures show almost the universal N_L dependence of W_L and W_H . Thus, the asymmetrical broadening is almost independent of the surface orientation and strain in this study. Consequently, the asymmetrical broadening in this study is mainly attributable to the PCEs in 2D Si, because of the high crystal quality of the 2D Si without forming an a-Si, which is evaluated by HRTEM.²⁴⁾ As a result, the larger W_L values due to PCEs in 2D Si are considered to enhance the phonon-scattering-induced mobility reduction of carriers.¹⁸⁾

On the other hand, it is reported that the Raman properties of the 2D Si layer are also affected by the tensile strain of the Si/SiO₂ interface, which is caused by the thermal stress of SiO₂ on the 2D Si layer.²⁸⁾ Therefore, the experimental $\Delta\omega$ is mainly attributable to both the PCEs and tensile strain of the Si/SiO₂ interface. However, it is difficult to analyze the influence of the tensile strain of the Si/SiO₂ interface without the PCEs on the $\Delta\omega$ data at present. In order to evaluate this influence, it is necessary to change the tensile strain value of the Si/SiO₂ interface, by changing the thermal oxidation temperature for forming ETSOIs. The experimental $\Delta\omega$ is shown in Fig. 6(a). When $N_L > 10$ ($T_S > 2$ nm), the $\Delta\omega$ values in all substrates are almost the same as those of the thicker SOI; thus, the Raman peak is independent of N_L , which is also consistent with the ETSOI data with $T_S \geq 5$ nm reported by Uchida et al.⁵⁾ However, when $N_L < 6$, the $\Delta\omega$ values in all substrate structures suddenly increases with decreasing N_L , and are about

20 cm^{-1} at $N_L \approx 3$, which is almost the same as that of Si-nanocrystal with a diameter of 2.5 nm.¹⁶ In addition, Fig. 6(b) shows the T_S dependence of the Raman peak downshift $\Delta\omega$ of (100)-SOI and (110)-SOI, where $N_L < 8$. $\Delta\omega$ can be well fitted by the power law of T_S with the correlation coefficient of about 0.998, similar to the 0D Si.¹⁶ As a result,

$$\Delta\omega = \beta \left(\frac{a}{T_S} \right)^\gamma, \quad (1)$$

where $\beta = 22.1 \text{ cm}^{-1}$, $\gamma = 2.75$ in the (100) 2D Si, and a is the Si lattice constant.

The E_P values under the Raman peak conditions in the 2D Si are reduced by the E_P reduction rate of $\Delta E_P/E_P = \Delta\omega/520$, resulting in $\Delta E_P/E_P \approx 4\%$ at N_L of about 3 ($T_S = 0.25 \text{ nm}$) in the (100) 2D Si. In addition, in the case of the N_L dependence of $\Delta\omega$, the (100) and the (110) data show the universal relationship between $\Delta\omega$ and N_L ; thus, the N_L dependence of $\Delta\omega$ is independent of the surface orientation.

On the other hand, subtracting $\Delta\omega$ obtained using Eq. (1) from experimental SSOI $\Delta\omega$ data, the strain ε of (100)-SSOI can be obtained. However, it is necessary to consider the T_S variation δT_S in the 2D Si to evaluate ε , because $\Delta\omega$ strongly depends on T_S . Here, the $\Delta\omega$ variation $\delta(\Delta\omega)$ is considered to be due to δT_S , and thus can be given by $\delta(\Delta\omega)/\Delta\omega = \gamma\delta T_S/T_S$, using Eq. (1). According to the $\Delta\omega$ mapping data in a $10^4 \mu\text{m}^2$ area of (100) 2D Si at $T_S \approx 0.25 \text{ nm}$, δT_S is estimated to be about 0.2 nm in this study. Figure 6(c) shows the N_L dependence of strain of SSOIs estimated by considering δT_S . At $N_L \approx 4$, δT_S leads to ε variation; thus, ε varies from 0.6 to 1.2%. Therefore, ε behavior at $N_L < 10$ is not clear at present. However, strain is independent of N_L , when $N_L > 10$. Therefore, strain can be maintained to be almost the same as the initial value of 0.7%, when $N_L > 16$ ($T_S > 2 \text{ nm}$).

Assuming that the E_P of the 2D Si layer has almost the same Raman intensity distribution function of $I_R(E_P)$ shown in Fig. 3, the average v_{SAT} of the 2D Si layer with N_L (T_S) can be estimated as a function of the optical phonon energy E_P . That is,¹⁰

$$v_{\text{SAT}}(E_P) = \sqrt{\frac{8}{3\pi m_0} \frac{\int \sqrt{E_P} I_R(E_P) dE_P}{\int I_R(E_P) dE_P}}, \quad (2)$$

where m_0 is the free-electron mass.

Figure 7 shows the v_{SAT} of the 2D Si layer as a function of N_L estimated using Eq. (2). The v_{SAT} in all substrates gradually decreases with decreasing N_L at $N_L > 9$ ($T_S > 1 \text{ nm}$), and are rapidly reduced at a rate of 5% at $N_L \approx 3$ ($T_S = 0.25 \text{ nm}$), because of the rapidly reduced E_P in the 2D Si, as shown in Fig. 6(a). Moreover, the relationship between v_{SAT} and N_L is independent of the surface orientation. On the other hand, the lower v_{SAT} values of SSOI are attributable to the lower E_P , which is due to the tensile strain in strained Si. In addition, the low E_P is considered to induce the thermal conductivity reduction in 2D Si, which is similar to the 1D Si.¹⁷ Therefore, self-heating effects¹ due to the low thermal conductivity probably cause the current drivability reduction in future devices composed of 2D Si.

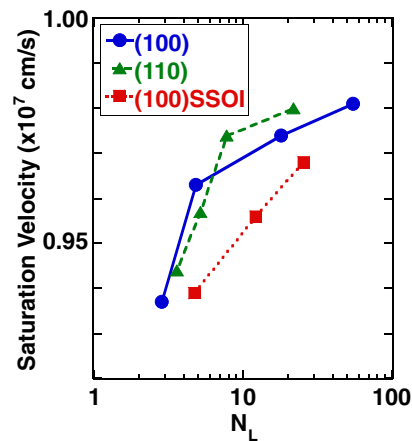


Fig. 7. (Color online) N_L dependence of the average v_{SAT} values of (100)-SOI (circles), (110)-SOI (triangles), and (100)-SSOI (squares) obtained using $v_{\text{SAT}} \propto E_P^{1/2}$ of Eq. (2). v_{SAT} rapidly decreases when $N_L < 8$. Moreover, the (100) and (110) 2D Si structures have the almost universal N_L dependence of v_{SAT} .

Consequently, the PCEs in 2D Si have the universal dependence of the number of Si atom layers, that is, they are independent of the Si surface orientation and strain. Therefore, these results indicate that, the PCEs of (110) 2D Si are larger than those of (100) 2D Si at the same T_S conditions, because $d_{110} > d_{100}$. The PCE-induced v_{SAT} reduction is one of the physical limitations of the 2D Si structures for realizing high-performance CMOS devices composed of the 2D Si structures.

3.2 PL characteristics of 2D Si structures

It is expected that PL characteristics strongly depend on the Si surface orientation, because only the (100) 2D Si layer is considered to be a direct band-gap structure.^{2,3,7} In this subsection, we discuss the experimental PL results of the 2D Si structures.

Figure 8(a) shows the emitted photon energy dependence of the PL spectra in the (100) and (110) 2D Si structures at various $h\nu$ values, where $T_S \approx 0.5 \text{ nm}$, that is, the N_L of the (100) and (110) 2D Si structures are about 5 and 4, respectively. When $h\nu \leq 2.81 \text{ eV}$, the PL spectra of the (100)-SOI and (100)-SSOI show very broad peaks (FWHM $\approx 0.3 \text{ eV}$) and are independent of $h\nu$, which are similarly found in Si photonic devices³ and p-Si.^{20,29} The peak photon energy E_{PH} under both $h\nu$ conditions is about 1.72 eV. On the other hand, the PL intensity I_{PL} of the (100)-SSOI is lower than that of the (100)-SOI, which suggests that PL intensity depends on the strain-induced band modulation in 2D Si. However, the PL spectrum at $h\nu = 3.81 \text{ eV}$ shows very sharp peak (FWHM $\approx 0.013 \text{ eV}$) and can be fitted by the three peak energies of P1 to P3.²⁴ In addition, the E_{PH} value of 1.85 eV at $h\nu = 3.81 \text{ eV}$ is higher than that at $h\nu \leq 2.81 \text{ eV}$. Therefore, these PL data suggest that the PL mechanism strongly depends on the excitation photon energy $h\nu$. On the other hand, we cannot detect the clear PL peak from the (110) 2D Si, which is probably due to the fact that optical transition in (110)-SOI with $T_S \approx 0.5 \text{ nm}$ is still indirect.^{3,7} Moreover, even in the (100) 2D Si structures, we cannot observe the PL spectra when T_S is larger than the critical value of T_S (T_{SC}). T_{SC} strongly

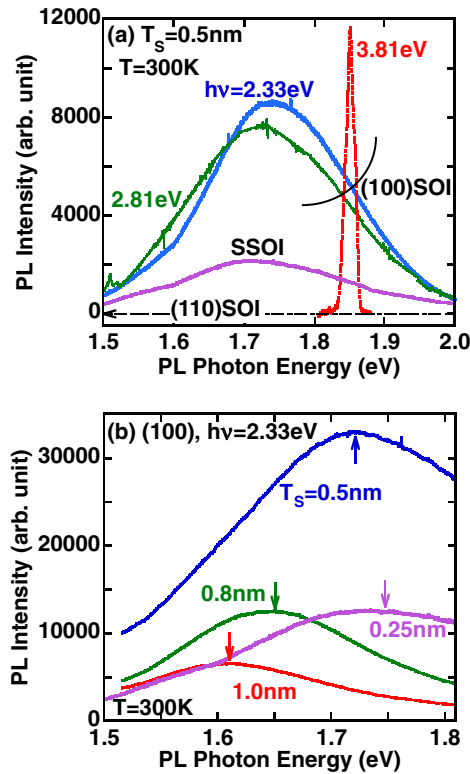


Fig. 8. (Color online) (a) PL photon energy dependence of PL spectra of (100)-SOI, (110)-SOI, and (100)-SSOI at $T_S \approx 0.5$ nm, where the lattice temperature T is 300 K, and $2.33 \leq h\nu \leq 3.81$ eV. We cannot detect the PL intensity of (110)-SOIs. The PL peak is very sharp only at $h\nu = 3.81$ eV; in the contrast the PL spectra at other $h\nu$ values are very broad. However, the PL spectrum at $h\nu = 2.81$ eV is almost the same as that at $h\nu = 2.33$ eV. (b) T_S dependence of PL spectra at $h\nu = 2.33$ eV vs PL photon energy of (100)-SOI; the arrows show the peak PL energy E_{PH} at various T_S values, where $0.25 \leq T_S \leq 1.0$ nm. I_{PL} and E_{PH} depend on T_S .

depends on $h\nu$, and the T_{SC} values at $h\nu \leq 2.81$ eV and $h\nu = 3.81$ eV are about 1 nm ($N_L \approx 9$) and 6 nm²⁴⁾ ($N_L \approx 45$), respectively. Consequently, in this work, we can observe the PL spectra of only the (100)-surface 2D Si with the direct band-gap structures including the SOI and SSOI substrates.

Moreover, Fig. 8(b) shows the T_S dependence of the PL spectra of the (100)-SOI, where $h\nu = 2.33$ eV. E_{PH} and I_{PL} strongly depend on T_S . Namely, I_{PL} rapidly increases with decreasing T_S , but I_{PL} also decreases at $T_S \approx 0.25$ nm. On the other hand, E_{PH} continues to increase with decreasing T_S .

Here, Fig. 9 shows a summary of the T_S dependence of the peak I_{PL} of the (100)-SOI, (110)-SOI, and (100)-SSOI at $h\nu = 2.33$ eV. In the case of the (110)-SOI, we cannot observe PL at $T_S \geq 0.5$ nm. The I_{PL} at $h\nu = 2.33$ eV of (100)-SOI rapidly increases with decreasing T_S in the case of $T_S \leq 1.0$ nm ($N_L < 10$), but I_{PL} also decreases at $T_S \approx 0.25$ nm ($N_L \approx 3$). When $T_S \geq 0.5$ nm in the (100)-SOI, I_{PL} is considered to be proportional to the excitation laser photon flux I_{FA} absorbed in the 2D Si layer with T_S ; thus, the I_{FA} can be expressed as follows¹⁰⁾

$$I_{PL} \propto I_{FA} = I_0(1 - R) \left\{ 1 - \exp \left[-\frac{T_S}{\lambda_P(T_S)} \right] \right\} = I_0(1 - R) \{ 1 - \exp[-\alpha(T_S)T_S] \}, \quad (3)$$

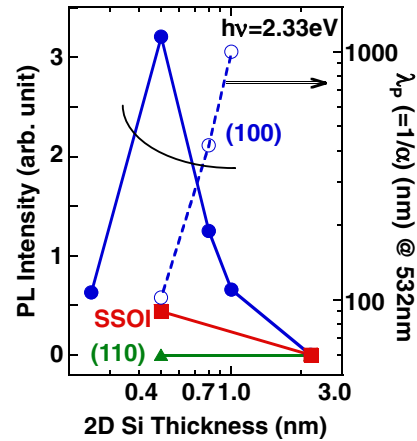


Fig. 9. (Color online) PL peak intensity I_{PL} of (100)-SOI (circles), (110)-SOI (triangles), and (100)-SSOI (squares) as a function of T_S , where T is 300 K and $h\nu = 2.33$ eV. I_{PL} of (100)-SOI rapidly increases at $T_S \leq 1$ nm, but decreases at $T_S = 0.25$ nm again. Moreover, I_{PL} of (100)-SSOI is very low. The right vertical axis shows the estimated λ_P [$\equiv 1/\alpha$ (α is the absorption coefficient)] of (100)-SOI (open circles) at $h\nu = 2.33$ eV, and the dashed line indicates that $\lambda_P \propto T_S^{3.2}$.

where I_0 is the photon flux at the Si surface, R is the reflectivity at the Si surface, λ_P is the penetration length in Si, and α is the absorption coefficient of the 532 nm photon in the Si layer. In order to explain the rapid increase in the I_{PL} of the (100) 2D Si shown as closed circles in Fig. 9, it is expected that the λ_P of (100) 2D Si at 532 nm laser wavelength strongly depends on T_S , and rapidly decreases with decreasing T_S . Using Eq. (3) and assuming that the R in Eq. (3) is independent of T_S , λ_P can be obtained as a function of T_S , shown as open circles in Fig. 9, and the λ_P at T_S of 0.5 nm is about one order of magnitude lower than that at T_S of 1.0 nm, resulting in $\lambda_P \propto T_S^{3.2}$. Very short λ_P , that is, very large α in the 2D Si is very suitable for a Si photonic device. These data strongly indicate the optical direct-transitions in the (100) 2D Si, because λ_P is reduced in the case of direct optical transitions.¹⁰⁾ However, in order to confirm the above-mentioned short λ_P in 2D Si, it is necessary to evaluate the α spectrum of 2D Si directly, using a Si-on-quartz (SOQ) substrate.

Next, Fig. 10 shows the T_S dependence of the PL peak photon energy E_{PH} of (100) 2D Si at $T = 300$ K. The E_{PH} at $h\nu = 2.33$ eV increases with decreasing T_S and is independent of the strain, which suggests that the E_G of 2D Si layer expands with decreasing T_S . Assuming the infinite confining SiO_2 potential, the analytical model of E_G as a function of T_S (dotted line in Fig. 10) is given as $E_G(T_S) = E_{G0} + 2h^2/T_S^2(m_L^*{}^{-1} + m_{HH}^*{}^{-1})$,²²⁾ where E_{G0} is the band-gap of 3D Si, and m_L^* ($\equiv 0.98m_0$) and m_{HH}^* ($\equiv 0.49m_0$) are the effective masses of electrons and heavy holes, respectively.¹⁰⁾ However, Fig. 10 shows that the experimental E_{PH} values in this work are smaller than the theoretical results (dotted and dashed line),⁷⁾ the analytical model, and reported data³⁰⁾ on E_G , whereas the experimental E_{PH} value at T_S of 1 nm is almost the same as the theoretical one.⁷⁾ In addition, the E_G deviation between our results and these reference data increases with decreasing T_S , and especially the E_G deviation becomes larger in the case of the analytical model. The physical mechanism for the E_G deviation is not

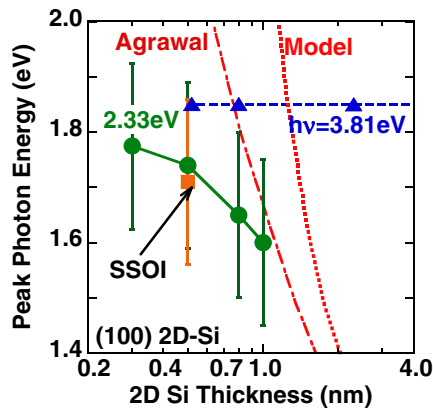


Fig. 10. (Color online) T_S dependence of PL peak photon energy of (100) 2D Si at $T = 300$ K. Circles and triangles show the results of (100)-SSOI at $h\nu = 2.33$ and 3.81 eV, respectively. Square shows the result of (100)-SSOI at $h\nu = 2.33$ eV. Error bars indicate the E_{PH} (0.15 eV) values estimated from the FWHM values of the PL spectra shown in Fig. 8. The dotted/dashed and the dotted lines show the theoretical⁷⁾ and the analytical²²⁾ results on T_S dependence of E_G of (100) 2D Si, respectively. The E_{PH} at $h\nu = 2.33$ eV increases with decreasing T_S , and the deviation between the experimental and the reference data also increases with decreasing T_S . In the contrast, the E_{PH} at $h\nu = 3.81$ eV remains constant at 1.85 eV.

understood at present, but the E_G graded region (about 0.2 nm in length) at the SiO_2/Si interface, that is, from a small E_G of the 2D Si layer to large E_G of the SiO_2 layers,³¹⁾ possibly causes the reduction of the quantum confinement effects in the 2D Si layer, resulting in our smaller E_G values. Consequently, the PL mechanism at $h\nu = 2.33$ eV is considered to be due to the direct optical transition of electron/hole pairs generated in 2D Si, as similarly found in the p-Si¹⁸⁾ and Si photonic devices.³⁾ On the other hand, the E_{PH} at $h\nu = 3.81$ eV is independent of T_S , and remains constant at 1.85 eV.²³⁾ Thus, the physical mechanism for the PL at $h\nu \leq 2.81$ eV is much different from that for the PL at $h\nu = 3.81$ eV. In our previous paper,²⁴⁾ we introduced a possible three-region model^{21,22)} for the PL mechanism at $h\nu = 3.81$ eV.

Here, we have introduced a simple model for the PL mechanism as function of high and low excitation photon energies. The above PL results are attributable to both the excess energy E_{EX} of the electrons generated at the Γ point of the 2D Si layers and the position difference of the emitted photons due to the recombination of electron/hole pairs. Namely, PL intensity strongly depends on $E_{EX} = h\nu - E_\Gamma$, where E_Γ is the energy level at the Γ point of (100) 2D Si and is equal to about 2 eV.³⁾ Figures 11(a) and 11(b) show the schematic band diagrams from the surface oxide to BOX layers for $h\nu \gg E_\Gamma$ and $h\nu \approx E_\Gamma$ cases, respectively. The surface and the back side interfaces between SiO_2 and Si show the E_G transition region.³¹⁾ In both $h\nu$ cases, the $\alpha(T_S)$ of the excitation photon in 2D Si rapidly increases with decreasing T_S , as shown in Fig. 8. In the interface regions, at least three energy levels from P1 to P3 exist, and the P1 level is the minimum value and the P3 level is the maximum value, according to our previous PL results.²⁴⁾ When $h\nu \gg E_\Gamma$ ($E_{EX} \gg 0$), as shown in Fig. 11(a), electrons generated by photons with a high energy of 3.81 eV become hot and can be injected into the

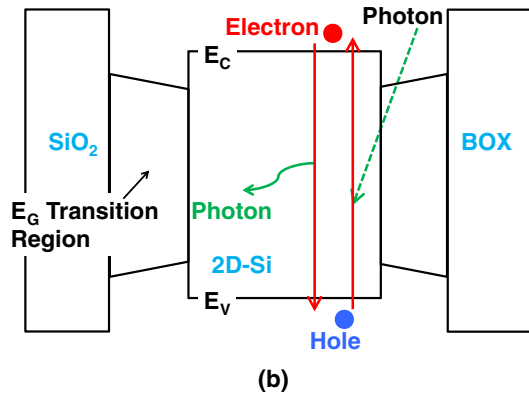
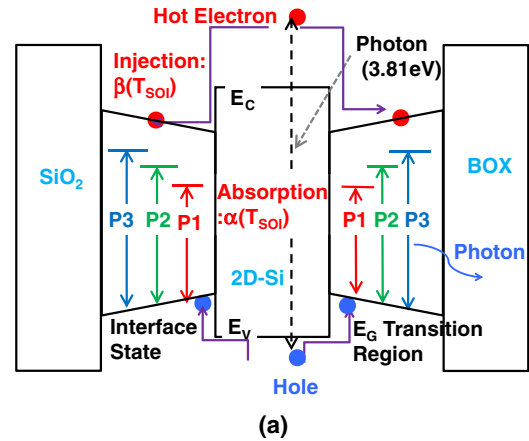


Fig. 11. (Color online) Schematic PL models for 2D Si layers in the case of excitation laser energies of (a) $h\nu = 3.81$ and (b) $h\nu < 3.81$ eV, using a three-region model.²⁴⁾ (a) When $h\nu = 3.81$ eV $\gg E_\Gamma$ [E_Γ (~ 2 eV) is the direct bandgap energy at Γ point of (100) 2D Si],²⁾ hot electron/hole pairs are generated in 2D Si layer, which are injected into the Si/SiO_2 interface E_G transition region.³⁰⁾ Hot carriers recombine at the Si/SiO_2 interface, where $\alpha(T_S)$ and $\beta(T_S)$ are the absorption coefficient of the excitation photons in 2D Si and the injection coefficient of hot electrons into the interfaces, respectively. (b) When $h\nu = 2.33/2.81$ eV $\approx E_\Gamma$, the generated electron/hole pairs directly recombine in a 2D Si layer with a direct band-gap.

E_G transition region at the SiO_2/Si interface, where the injection coefficient $\beta(T_S)$ depends on E_{EX} . At the E_G transition interface regions, the photons are emitted by the recombination of generated electron/hole pairs.²⁴⁾ As a result, the E_{PH} at $h\nu = 3.81$ eV is proportional to $(E_1 - E_V)$ and is thus independent of the E_G of 2D Si, where E_1 and E_V are interface state energy levels with the three different values (P1 to P3) and the valence band levels, respectively. On the other hand, when $h\nu \approx E_\Gamma$ ($E_{EX} \approx 0$), as shown in Fig. 11(b), electron/hole pairs are generated by excitation photons with a relatively low energy, and thus do not become hot. Therefore, since generated electron/hole pairs are directly recombined in the 2D Si region with the direct band-gap structures, the photons are emitted directly in the 2D Si layers, resulting in $E_{PH} \approx E_\Gamma$. As a result, E_{PH} strongly depends on the T_S of 2D Si, because E_Γ and the band structures of 2D Si strongly depend on T_S .

Consequently, we have demonstrated the excitation photon energy dependence of the PL phenomena in the 2D Si layers, which can be qualitatively explained by the simple

PL model. In addition, the PL results strongly depend on the surface orientation of the 2D Si layers, whereas the phonon confinement effects are independent of the surface orientation, as discussed in the previous section. This is because the band structures of 2D Si strongly depend on the surface orientation.

4. Conclusions

We have experimentally studied the surface orientation/tensile-strain effects on quantum mechanical confinements (QMCs) in 2D Si layers for future CMOS devices, using (100)-SOI, (110)-SOI, and (100)-SSOI substrates. Because of the rapid increase of the UV-Raman intensity with decreasing 2D Si thickness T_S and number of Si atom layer N_L , which is attributable to the resonant Raman scattering, we can evaluate in detail the phonon properties of the 2D Si by UV-Raman spectroscopy, even at $T_S < 0.5$ nm ($N_L < 5$). We have demonstrated that the quantum phonon confinement effects (PCEs), including the asymmetric broadening of the Raman line shapes and the Raman peak downshift, enhance with decreasing T_S and N_L , but the N_L dependence of the PCEs is almost independent of the surface orientation and tensile strain. Therefore, the N_L dependence instead of the T_S dependence is the better indicator for evaluating the Raman characteristics of 2D Si phonons. As a result, we found that the phonon energy of 2D Si decreases with decreasing T_S , that is, N_L , which is mainly caused by the PCEs of the 2D Si structures. Thus, the carrier saturation velocity in the 2D Si structures is estimated to be reduced by a low phonon energy.

On the other hand, we can observe photoluminescence (PL) characteristics of the (100) 2D Si layers, but we cannot detect the PL of the (110) 2D Si. This is because the band structures strongly depend on the surface orientation. Namely, (100) 2D Si has direct band-gap structure, but in the contrast (110) 2D Si has the usual indirect band-gap structure. In addition, the PL spectra of (100) 2D Si strongly depends on the excitation photon energy $h\nu$ in the range of $2.33 \leq h\nu \leq 3.81$ eV, which can be qualitatively explained by the simple PL models considering the excess energy of generated electrons in the 2D Si layers. Namely, when the $h\nu$ is high ($h\nu = 3.81$ eV), the PL peak photon energy E_{PH} of 1.85 eV is independent of T_S , which is attributable to the recombination of the generated hot electron/hole pairs in the graded band-gap regions at the SiO₂/Si interface region. On the other hand, in the case of a lower $h\nu$ ($h\nu \leq 2.81$ eV), E_{PH} increases with decreasing T_S , because the generated electron/hole pairs directly recombine in the 2D Si layers. PL intensity increases with decreasing T_S , which suggests the rapid reduction in the absorption coefficient of photons in the 2D Si. Consequently, it is necessary to reconstruct the device design for future planar and 3D CMOS devices, such as ETSOI-CMOS and FinFETs composed of 2D Si structures, considering the above PCEs and the band structure modulation.

Acknowledgements

We would like to thank Professor J. Nakata and Dr. Y. Hoshino of Kanagawa University for the thermal oxidation process of Si. This work was partially supported by a Grant-in-Aid for Scientific Research from the Japan Society for the Promotion of Science (24560422).

- 1) A. Nazarov, J.-P. Colinge, F. Balestra, J.-P. Raskin, F. Gamiz, and V. S. Lysenko: *Semiconductor-On-Insulator Materials for Nanoelectronics Applications* (Springer, Berlin, 2011).
- 2) S. Saito, D. Hisamoto, H. Shimizu, H. Hamamura, R. Tsuchiya, Y. Matsui, T. Mine, T. Arai, N. Sugii, K. Torii, S. Kimura, and T. Onai: *Jpn. J. Appl. Phys.* **45** (2006) L679.
- 3) S. Saito, N. Sakuma, Y. Suwa, H. Arimoto, D. Hisamoto, H. Uchiyama, J. Yamamoto, T. Sakamizu, T. Mine, S. Kimura, T. Sugawara, M. Aoki, and T. Onai: *IEDM Tech. Dig.*, 2008, Paper 19.5.
- 4) K. Uchida, H. Watanabe, A. Kinoshita, J. Koga, T. Numata, and S. Takagi: *IEDM Tech. Dig.*, 2002, p. 47.
- 5) K. Uchida, J. Koga, and S. Takagi: *J. Appl. Phys.* **102** (2007) 074510.
- 6) G. Tsutsui, M. Saitoh, and T. Hiramoto: *IEEE Trans. Electron Devices* **26** (2005) 836.
- 7) B. K. Agrawal and S. Agrawal: *Appl. Phys. Lett.* **77** (2000) 3039.
- 8) M. Tabe, M. Kumezawa, and Y. Ishikawa: *Jpn. J. Appl. Phys.* **40** (2001) L131.
- 9) Z. H. Lu and D. Grozea: *Appl. Phys. Lett.* **80** (2002) 255.
- 10) S. M. Sze and K. K. Ng: *Physics of Semiconductor Devices* (Wiley, New York, 2006).
- 11) N. Fukata, T. Oshima, K. Murakami, T. Kizuka, T. Tsurui, and S. Ito: *J. Appl. Phys.* **100** (2006) 024311.
- 12) K. W. Adu, H. R. Gutierrez, and P. C. Eklund: in *Nanosilicon*, ed. V. Kumar (Elsevier, Oxford, U.K., 2008) Chap. 7.
- 13) H. Richter, Z. P. Wang, and L. Ley: *Solid State Commun.* **39** (1981) 625.
- 14) I. H. Campbell and P. M. Fauchet: *Solid State Commun.* **58** (1986) 739.
- 15) L. Khriachtchev, M. Rasanen, S. Novikov, O. Kilpela, and J. Sinkkonen: *J. Appl. Phys.* **86** (1999) 5601.
- 16) G. Faraci, S. Gibilisco, P. Russo, and A. R. Pennisi: *Phys. Rev. B* **73** (2006) 033307.
- 17) S. Piscanec, M. Cantoro, A. C. Ferrari, J. A. Zapien, Y. Lifshitz, S. T. Lee, S. Hofmann, and J. Robertson: *Phys. Rev. B* **68** (2003) 241312(R).
- 18) L. Donetti, F. Gámiz, J. B. Roldán, and A. Godoy: *J. Appl. Phys.* **100** (2006) 013701.
- 19) S. S. Iyer and Y.-H. Xie: *Science* **260** (1993) 40.
- 20) A. G. Cullis, L. T. Canham, and P. D. J. Calcott: *J. Appl. Phys.* **82** (1997) 909.
- 21) T. Sameshima, H. Watakabe, N. Andoh, and S. Higashi: *Jpn. J. Appl. Phys.* **45** (2006) 2437.
- 22) Y. Takahashi, T. Furuta, Y. Ono, T. Ishiyama, and M. Tabe: *Jpn. J. Appl. Phys.* **34** (1995) 950.
- 23) A. D. Lan, B. X. Liu, and X. D. Bai: *J. Appl. Phys.* **82** (1997) 5144.
- 24) T. Mizuno, K. Tobe, Y. Maruyama, and T. Sameshima: *Jpn. J. Appl. Phys.* **51** (2012) 02BC03.
- 25) T. Mizuno, K. Higa, Y. Nakajima, D. Urata, Y. Abe, H. Akamatsu, Y. Nagata, Y. Nakahara, Y. Sato, J. Takehi, and T. Sameshima: *Ext. Abstr. Solid State Devices and Materials*, 2012, p. 829.
- 26) Web [http://www.silvaco.com].
- 27) J. B. Renucci, R. N. Tyte, and M. Cardona: *Phys. Rev. B* **11** (1975) 3885.
- 28) H. Omi, T. Kawamura, S. Fujikawa, Y. Tsusaka, Y. Kagoshima, and J. Matsui: *Appl. Phys. Lett.* **86** (2005) 263112.
- 29) Y. K. Xu and S. Adachi: *J. Appl. Phys.* **107** (2010) 123520.
- 30) D. J. Lockwood, Z. H. Lu, and J.-M. Baribeau: *Phys. Rev. Lett.* **76** (1996) 539.
- 31) Y. Yamashita, S. Yamamoto, K. Mukai, J. Yoshinobu, Y. Harada, T. Tokushima, T. Takeuchi, Y. Takata, S. Shin, K. Akagi, and S. Tsuneyuki: *Phys. Rev. B* **73** (2006) 045336.